nanomaterials

MDPI

Article

On Thermal Distribution for Darcy–Forchheimer Flow of Maxwell Sutterby Nanofluids over a Radiated Extending Surface

Wen Wang [1], Mohammed M. M. Jaradat [2,*], Imran Siddique [3,*], Abd Allah A. Mousa [4], Sohaib Abdal [5,6], Zead Mustafa [2] and Hafiz Muhammad Ali [7,8,*]

1 College of Mechanical Engineering, Xijing University, Xi'an 710123, China; wangwen2227@163.com
2 Mathematics Program, Department of Mathematics, Statstics and Physics, College of Arts and Sciences, Qatar University, Doha P.O. Box 2713, Qatar; zead@qu.edu.qa
3 Department of Mathematics, University of Management and Technology, Lahore 54770, Pakistan
4 Department of Mathematics and Statistics, College of Science, Taif University, P.O. Box 11099, Taif 21944, Saudi Arabia; a.mousa@tu.edu.sa
5 School of Mathematics, Northwest University, No. 229 North Taibai Avenue, Xi'an 710069, China; sohaib@stumail.nwu.edu.cn
6 Department of Mathematics, Khawaja Fareed University of Engineering and Information Technology, Rahim Yar Khan 64200, Pakistan
7 Mechanical Engineering Department, King Fahd University of Petroleum & Minerals, Dhahran 31261, Saudi Arabia
8 Interdisciplinary Research Center for Renewable Energy and Power Systems (IRC-REPS), King Fahd University of Petroleum and Minerals, Dhahran 31261, Saudi Arabia
* Correspondence: mmjst4@qu.edu.qa (M.M.M.J.); imransmsrazi@gmail.com (I.S.); hafiz.ali@kfupm.edu.sa (H.M.A.)

Citation: Wang, W.; Jaradat, M.M.M.; Siddique, I.; Mousa, A.A.A.; Abdal, S.; Mustafa, Z.; Ali, H.M. On Thermal Distribution for Darcy–Forchheimer Flow of Maxwell Sutterby Nanofluids over a Radiated Extending Surface. *Nanomaterials* **2022**, *12*, 1834. https://doi.org/10.3390/nano12111834

Academic Editor: Mikhail Sheremet

Received: 9 February 2022
Accepted: 3 March 2022
Published: 27 May 2022

Abstract: This study addresses thermal transportation associated with dissipated flow of a Maxwell Sutterby nanofluid caused by an elongating surface. The fluid passes across Darcy–Forchheimer sponge medium and it is affected by electromagnetic field applied along the normal surface. Appropriate similarity transforms are employed to convert the controlling partial differential equations into ordinary differential form, which are then resolved numerically with implementation of Runge–Kutta method and shooting approach. The computational analysis for physical insight is attempted for varying inputs of pertinent parameters. The output revealed that the velocity of fluid for shear thickening is slower than that of shear thinning. The fluid temperature increases directly with Eckert number, and parameters of Cattaneo–Christov diffusion, radiation, electric field, magnetic field, Brownian motion and thermophoresis. The Nusselt number explicitly elevated as the values of radiation and Hartmann number, as well as Brownian motion, improved. The nanoparticle volume fraction diminishes against Prandtl number and Lewis number.

Keywords: Sutterby fluid; Darcy–Forchheimer; electric field; nanofluid; Maxwell fluid; Cattaneo–Christov diffusion

1. Introduction

The fluids whose viscosity varies non-linearly because of applied stress are referred to as non-Newtonian fluids. Examples of some of these liquids in real-life are ketchup, semen, honey, wax, jellies, etc. Over the last several years, research concerning non-Newtonian fluids has been greatly enhanced owing to their functional effects for technology and manufacturing processes. Analysis on change of viscosity, and thus the behavior of non-Newtonian fluids, was conducted by Shende et al. [1]. The heat transmit by forced convection of a non-Newtonian liquid in a fractional constitutive version boundaries based on a pipe was examined by Chang et al. [2]. For the result of non-Newtonian fluid flow, simulations for the time-lattice for Boltzmann process paradigm were taken

by Bisht et al. [3]. Abu et al. [4] analyzed the viscous blend of non-Newtonian fluid in the presence of turbulent flow along with vapor bubble growth. The radiative flow deep research with MHD in signification of non-Newtonian fluids by incorporating the most recent version of the heat flow rate model. By using the modified version of the heat flow rate model, the radiative flowing deep analysis with magnetohydrodynamic on the nature of non-Newtonian fluids was taken by Sohail et al. [5]. Examples of researchers work on non-Newtonoan fluid subject to various types of geometries can be found in [6–9]. The porous media engagement has significant wide range of applications in the zone of heat transfer design, geothermal, geophysics, under ground water system, recovery system of crude oil, and units of energy storages [10,11]. Ali et al. [12] analyzed the Darcy–Forchheimer medium impacts on the dynamic of nanofluid flow.

The rheological phenomena of non-Newtonian viscosity varying with yields time elastic results pertaining to polymer methods as well as polymer melt. Sutterby fluid, which signifies constitutive equations for extremely polymer aqueous solutions, is one of the most crucial non-Newtonian fluids. To facilitate economic output efficiency, the Sutterby fluid that defines the strictly viscous behavior of the non-Newtonian is known. Scholars are putting their efforts to reveal the properties of Sutterby fluid such as Akram et al. [13], who studded deeply in the presence of electromagnetic fields the Sutterby fluid model which is blood-based graphene oxide nanofluid flows through capillary. Salahuddin et al. [14] examined the dynamics of Sutterby fluid subject to catalytic parabolic surface. Hayat et al. [15] examined the impact of fluid stream from Sutterby and found that it is prone to homogeneous-heterogeneous as well as nonlinear radiation transformations. Nawaz et al. [16] discussed the function of hybrid nanoparticles throughout the thermal efficiency of ethylene glycol, the Sutterby fluid. Thermal and energy stratified flow analysis of Sutterby nanofluid with zero mass flux status was taken by Mir et al. [17]. Sabir et al. [18] examined the consequences of heat radiation and inclined magnetic force on the Sutterby fluid employing the Cattaneo–Christov thermal gradient scheme.

Nanofluids are possible heat storage liquids with enhanced thermos-physical characteristics, so analytical platforms for optimized illustrations may be associated through heat trading activity. Study nowadays in the domain of nanomaterials has quickly evolved influencing to its extensive deployments in various areas, due to its wide range uses, such as thermal transportation. Many intellectuals have paid too much attention to the new aspects in this domain. Mahdavi et al. [19] extensively reviewed nanofluid jet refrigerating fluid motion and heat transition assessment on a hot exterior with variable roughness. Stability analysis of nanofluids was carried out by Chakraborty et al. [20]. Esfe et al. [21] explored nanofluids streamline for enhanced oil recovery in kind of a heterogeneous two-dimensional anticline geometry. Swaim et al. [22] demonstrated a comprehensive inspection into the impacts of accelerating heating source across an inclined magnetic flux. Many researchers also explored nanofluids in different areas [23–27].

It is possible to find strong energy throughout the domain of nanofluids. They can also be used to determine the effects of calming stress. A description of fluids of the pressure pattern, viz., the model of Maxwell will predict stress relief and has become much more general instead. The research of Maxwell flow of nanofluid has grown substantially in latest generations leading to several applications in engineering including medical processes. Sharma et al. [28] numerically studied the Maxwell nanofluid graphene flows past a uniformly stretched sheet. Maxwell base fluid stream including magnetohydrodynamic dissipative and radiative graphene was taken by Hussain et al. [29]. Abro et al. [30] analyzed the thermophysical characteristics of Maxwell nanofluids with normal kernel through fractional derivatives. A mathematical and statistical approach to the effect of radiative heat flux in Maxwell flow of viscoastic fluid over a chemically reacted spiraling disc was carried out by Ahmad et al. [31]. Microstructure-like substantial flowing along with bio-convection with inertial properties of Magnetohydrodynamic suspended SWCNT- and MWCNT-dependent Maxwell nanofluid examined by Shah et al. [32]. Ali et al. [33] re-

viewed gyrotactic microorganisms Falkner–Skan flow of Maxwell nanofluid with activation energy above a wedge.

From the above literature the authors discovered that the thermal distribution for transportation of Darcy–Forchheimer Maxwell Sutterby nanofluid flow in the availability of Cattaneo–Christov heat transition and electromagnetic field is rarely taken into account. Furthermore, the use of convective boundary conditions and bio-convection of microbes enhances to the innovation of this research. Because of the pairing and higher order non-linearity of the governing boundary value problem, arithmetical findings are achieved by conducting the Runge–Kuttta strategy code with shooting notion on the Matlab program. The findings are affirmed as a specific situation of prior findings.

2. Mathematical Formulation

By considering dissipated Darcy–Forchheimer multi-slip constraints over a time-independent flow of Maxwell Sutterby nanofluid. A two-dimensional electro- and magnetohydrodynamic boundary with the presence of Lorentz force [34] and incompressible Maxwell Sutterby fluid is defined as $F = \sigma_m(E_f + (J_1 * B_0))$.

A base is extended with velocity $U_w(x) = a_1 x$ along boundary. On the surface of the layer, a constant T_w temperature is provided in vertical direction, a magnetic flux of intensity B_0 is imposed upon this flow (see Figure 1). According to the above-mentioned assumption, the governing equations are [35–37]

$$\frac{\partial u}{\partial x} + \frac{\partial v}{\partial y} = 0, \tag{1}$$

$$u\frac{\partial u}{\partial x} + v\frac{\partial u}{\partial y} = \frac{\nu}{2}\frac{\partial^2 u}{\partial y^2}(1 + \frac{Sb_c^2}{2}(\frac{\partial u}{\partial y})^2) + \frac{\sigma_m B_0}{\rho}(E_f - B_0 u) - \frac{\nu}{k'}u \tag{2}$$
$$-\lambda_1[u^2\frac{\partial^2 u}{\partial x^2} + v^2\frac{\partial^2 u}{\partial y^2} + 2uv\frac{\partial^2 u}{\partial y \partial x}] - \frac{C_F^*\sqrt{k'}}{\nu}u^2,$$

$$u\frac{\partial T}{\partial x} + v\frac{\partial T}{\partial y} = \frac{k_1}{\rho C_p}\frac{\partial^2 T}{\partial y^2} + \frac{\rho_p C_p}{\rho C}[D_B\frac{\partial C}{\partial y}\frac{\partial T}{\partial y} + \frac{D_T}{T_\infty}(\frac{\partial T}{\partial y})^2] \tag{3}$$
$$+\frac{\mu}{\rho C_p}(\frac{\partial u}{\partial 2})^2 - \frac{1}{\rho C_p}\frac{\partial q_r}{\partial y} + \frac{\sigma_2}{\rho C_p}(uB_0 - E_f)^2 - \tau_1 B^*,$$

$$u\frac{\partial C}{\partial x} + v\frac{\partial C}{\partial y} = D_B\frac{\partial}{\partial y}\frac{\partial C}{\partial y} + \frac{D_T}{T_\infty}\frac{\partial}{\partial y}\frac{\partial T}{\partial y}. \tag{4}$$

$$B^* = [u\frac{\partial u}{\partial x}\frac{\partial T}{\partial x} + v\frac{\partial v}{\partial x}\frac{\partial T}{\partial x} + u\frac{\partial v}{\partial x}\frac{\partial T}{\partial x} + v\frac{\partial u}{\partial y}\frac{\partial T}{\partial x} + 2uv\frac{\partial^2 T}{\partial x \partial y} + u^2\frac{\partial}{\partial x}\frac{\partial T}{\partial x} + v^2\frac{\partial}{\partial y}\frac{\partial T}{\partial y}].$$

Here, u and v represent the component of velocity in x- and y-direction, respectively; the flow deportment index is S; b_c^2 represents consistency index; σ_m is the magnetic permeability; ρ signifies density; electric field strength is E_f; C_F^* symbolizes Forchheimer quantity; T represents temperature; C indicates solutal density; k_1 represents thermal conductivity; C_p signifies specific heat; τ_1 is heat relaxation time; $q_r = (\frac{-4T_\infty^3\sigma_m}{3k^{**}})\frac{\partial}{\partial y}T^4$ denotes radiative heat flux; C represents nanoparticles concentration; and Brownian motion constant is viewed by D_B and the thermophorsis constant is expressed by D_T.

The model's boundary situations are given below.

$$\left.\begin{aligned} u = U_w + N_0\frac{\partial u}{\partial y}, v = 0, T = T_w(x) + k_0\frac{\partial T}{\partial y}, C = C_w(x) + k_2\frac{\partial C}{\partial y}, \quad as \quad y = 0, \\ u \to 0, \quad T \to T_\infty, \quad C \to C_\infty, \quad as \quad y \to \infty. \end{aligned}\right\} \tag{5}$$

Here, $U_w = a_1 x, a_1 > 0$ denotes stretching velocity, T_∞ symbolizes ambient temperature, slip length is N_0, C_w designates wall concentration, C_∞ denotes ambient concentration, and k_0 signifies heat jump length and k_2 depicts the density jump length.

Using the similarity variables [33]

$$\eta = \sqrt{\frac{a}{\nu}}y, \psi = \sqrt{a\nu}xf(\eta),\ \theta(\eta) = \frac{T - T_\infty}{T_w - T_\infty},\ \phi(\eta) = \frac{C - C_\infty}{C_w - C_\infty}. \tag{6}$$

Substituting relation (6) in Equations (2)–(4), we get

$$f''' - 2f'^2 + 2ff'' - \beta(f^2f''' - 2ff'f'') - \frac{S}{2}ReDef''^2f''' + 2Ha^2(E_1 - f') - 2K_pf' - 2F_1^*f'^2 = 0, \tag{7}$$

$$\frac{1}{Pr}(1 + \frac{4}{3}Rd)\theta'' + f\theta' + Nb\theta'\phi' + Nt\theta'^2 - b(f^2\theta'' + ff'\theta') + Ecf''^2 + EcHa^2(f' - E_1) = 0, \tag{8}$$

$$\phi'' + PrLef\phi' + \frac{Nt}{Nb}\theta'' = 0. \tag{9}$$

where transformed boundary conditions (5),

$$\left.\begin{aligned} f(0) = 0,\ f'(0) = 1 + \delta f'',\ \theta(0) = 1 + \beta\theta',\ \phi(0) = 1 + \gamma\phi',\ at\ \eta = 0, \\ f'(\infty) \to 0,\ \theta(\infty) \to 0, \phi(\infty) \to 0,\ as\ \eta \to \infty. \end{aligned}\right\} \tag{10}$$

The non-dimensional factors are listed in the preceding order:

$\beta = \lambda a$ is Maxwell fluid Deborah number, $Ha = \sqrt{\frac{\sigma_m}{\rho}}B_0$ is the magnetic parameter, $Re = \frac{ax^2}{\nu}$ is the Reynolds number, Deborah number is $De = b^2a^2$, electric parameter is $E_1 = \frac{E_f}{xaB_0}$, porosity parameter is $Kp = \frac{\nu}{k'a}$, inertia parameter is $F_1^* = \frac{C_F^*}{\sqrt{k'}}$, Prandtl number is $Pr = \frac{\nu}{\alpha}$, radiation parameter is $Rd = \frac{16T_\infty^3\sigma_m}{3k^{**}\kappa}$, $Ec = \frac{a^2x^2}{C_p(T_w - T_\infty)}$ denotes Eckert number, $b = \tau_1 a$ is the constant of thermal relaxation, $Nb = \frac{\rho_pC_p}{\alpha\rho C}D_B(C_w - C_\infty)$ and $Nt = \frac{\rho_pC_pD_T(T_w - T_\infty)}{\alpha\rho CT_\infty}$ are Brownian motion and thermophoresis parameter, Lewis number is $Le = \frac{\nu}{D_B}$.

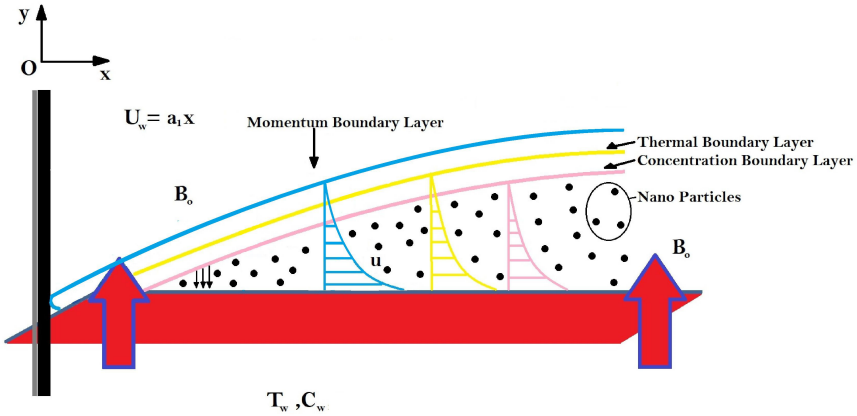

Figure 1. Problem description.

The physical quantities are signified as follows [38]:

Cf_x (skin friction coefficient), Nu_x (local Nusselt number), and Sh_x (local Sherwood number) are given below:

$$Cf_x = \frac{\tau_w}{\rho U^2 w},\ Nu_x = \frac{xq_w}{k_1(T_w - T_\infty)},\ Sh_x = \frac{xq_m}{D_B(C_w - C_\infty)},$$

where τ_w, q_w, and q_m denotes shear stress, surface heat flux and surface mass flux are given by (at $y = 0$),

$$\tau_w = -\mu[(1+\beta)\frac{\partial u}{\partial y} + \frac{Sb_c^2}{3}(\frac{\partial u}{\partial y})^3],\ q_w = -k_1\frac{\partial T}{\partial y},\ q_m = -D_B\frac{\partial C}{\partial y}$$

When we solve these quantities utilizing the assigned similarity transformation, we get

$$C_f(Re_x)^{-1/2} = -[(1+\beta)(f''(0) + \frac{S}{3}ReDef''(0)^3)],\ Nu_x(Re_x)^{-1/2} = -\theta'(0),\ Sh_x(Re_x)^{-1/2} = -\phi'(0),$$

where, $(Re_x) = \frac{xU_w}{\nu}$ signifies the local Reynolds number.

3. Solution Procedure

Numerical scheme is coded in Matlab software to get the graphical and tabular output. First-order scheme with just some factor implemented as shown below [39–42]:

$s_1' = s_2$
$s_2' = s_3$
$s_3' = (-1)[-2s_2^2 + 2s_1s_3 - \beta(s_1^2ds_3 - 2s_1s_2s_3) - \frac{S}{2}ReDes_3^2s_3' + 2Ha^2(E_1 - s_2) - 2K_ps_2 - 2F_1^*s_2^2]$
$s_4' = s_5$
$s_5'(\frac{1}{Pr}(1 + \frac{4}{3}Rd)) = (-1)[s_1s_5 + Nbs_5s_7 + Nts_5^2 - b(s_1^2\theta'' + s_1s_2s_5) + Ecs_3^2 + EcHa^2(s_2 - E_1)]$
$s_6' = s_7$
$s_7' = -PrLes_1s_7 - \frac{Nt}{Nb}ds_5$

along with the boundary conditions:

$$s_1 = 0,\ s_2 = 1 + \delta s_2,\ s_3 = h,\ s_4 = 1 + \beta s_4,\ s_5 = g,\ s_6 = 1 + \gamma s_6,\ s_7 = i, \text{at}\ \eta = 0$$
$$s_2 \to 0,\ s_4 \to 0,\ s_6 \to 0\ as\ \eta \to \infty.$$

The unknown initial conditions s_3, s_5, s_7, are allotted arbitrary values to begin the computational methodology once the solution validates the boundary conditions, these values are finalized.

4. Results and Discussion

The numerical procedure, as described in the above section, yielded a solution of the controlling equations. The dependent physical variables like temperature of fluid $\theta(\eta)$, velocity $f'(\eta)$, nanoparticle volume fraction $\phi(\eta)$, Nusselt number $-\theta'(0)$, skin friction factor $-f''(0)$ and Sherwood number $-\phi'(0)$. For appropriate variations of influential factors, the variable attitude of these parameters has been calculated. The current arithmetic coding is ascertained because there appears to be a satisfactory agreement between the current and previously existing outcomes (see Table 1).

Table 1. The comparative outputs for $-f''(0)$.

Ha	Ibrahim and Negera [35]	Sajid et al. [38]	Present Results
0.0	1.2105	1.1706	1.1917
0.3	1.3578	1.3393	1.3485
0.5	1.4478	1.4408	1.4456
1.0	1.6504	1.6677	1.6545

The graphs in Figures 2–10 are sketched for two cases of Sutterby fluid parameter S ($S = -0.5, S = 0.5$). Note that $S > 0$ is related to shear thickening and $S < 0$ indicates shear thinning. Note that the velocity $f'(\eta)$ for shear thinning is faster than that for shear thickening. Figure 2 displays the influence of Maxwell parameter β and electric parameter E_1 on $-f'(\eta)$. Both of these parameters have the potential to increase the flow speed. The impacts of porosity parameter Kp, Hartmann number Ha and inertia parameter F_1^* on

velocity $f'(\eta)$ are plotted in Figure 3. It is reviewed that the flow become faster when Ha is slightly intensified but it decelerates against the augmented values of Kp and F_1^*. Physically, the existence of the resistive force in the form of Lorentz force is due to the inclusion of enhancing external magnetic field and leads to deceleration of the velocity, but an opposite behavior is perceived for temperature distribution, and the porous medium interaction makes the fluid more viscous, which slows down the velocity. Figure 4 presents the varying pattern of fluid velocity when Deborah number De and Reynolds number Re are enhanced. Note that these parameters directly increase the velocity $f'(\eta)$ for shear thinning but retard the flow for shear thickening. The viscoelastic effects generate the resistance force which cause the profile of velocity to decline. Figure 5 displays a lowering of the fluid temperature $\theta(\eta)$ against Pr and an increase in $\theta(\eta)$ when radiation parameter Rd is promoted in value. The results in this figure can be explained on the basis of physical nature of the parameters Pr and Rd. The Prandtl number is related inversely to thermal diffusivity, its higher values are responsible for the diminishing temperature distribution. The large inputs of radiation parameter Rd means incremented radiative mode of heat and hence rise in temperature is attained.

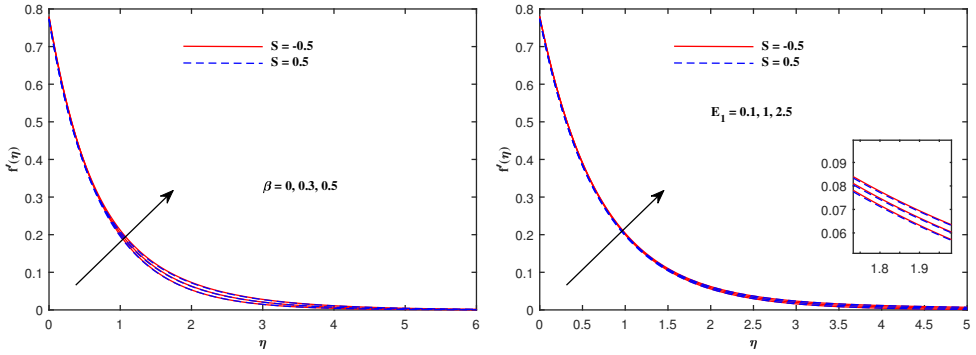

Figure 2. Velocity variation with β and E_1.

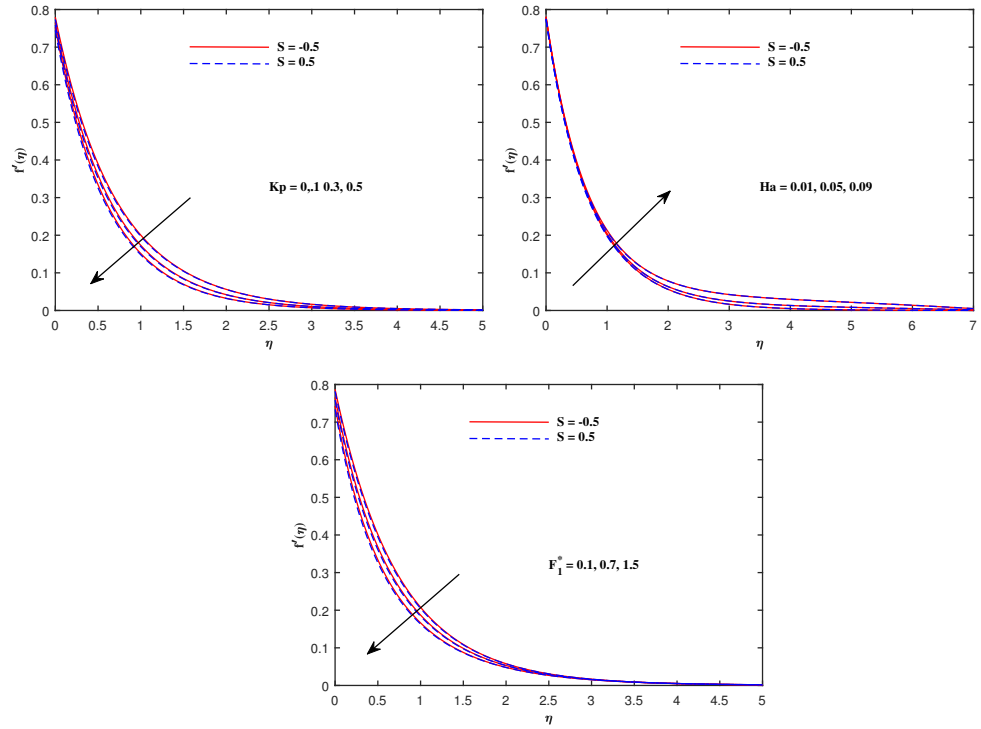

Figure 3. Velocity variation with Kp, Ha and F_1^*.

From Figure 6, it is depicted that the temperature increases when Nb and Nt increase. The faster Brownian movement and thermophorsis strengthen the thermal distribution.

The nanoparticles traveled from hot region to cold region due to thermophoretic force, and heat transfer rate is increased at the boundary surface. Similarly, faster movement of tiny particles raised the Brownian force, which boosts the base fluid temperature. In Figure 7, the plots for boosted temperature distribution are delineated with growing inputs of Cattaneo–Christov parameter b and Hartmann number Ha. A similar improved pattern of $\theta(\eta)$ are sketched in Figure 8, when Eckert number Ec and electric parameter E_1 are enhanced. The nanoparticle volume fraction $\phi(\eta)$ diminishes against Nb, but it enhances with higher values of Nt as noticed from Figure 9. Figure 10 reveal that the nanoparticle volume fraction $\phi(\eta)$ declines significantly against the growing values of Pr and Le. Table 2 identifies the skin friction coefficient $-f''(0)$, which declines with expanding Hartmann number Ha as well as Maxwell fluid factor β and although intensifies effectively with S, Re, De, Kp and F_1^*. The electric parameter E_1 does not make any mentionable effects on $-f''(0)$. The Nusselt quantity $-\theta'(0)$ enhances as the factors Rd, Ha as well as Nb are raised, but lowers when the variables Pr, b, Ec, E_1 and Nt are expanded, as revealed in Table 3. Table 4 portrays the accelerated advancement of the Sherwood quantity $-\phi'(0)$ if the values of Le as well as Nt are improved, and it lessens if the values of Pr as well as Nb are expanded.

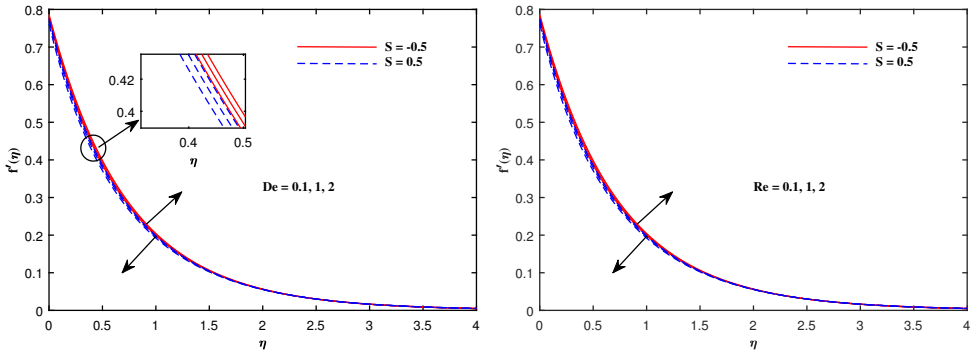

Figure 4. Velocity variation with De and Re.

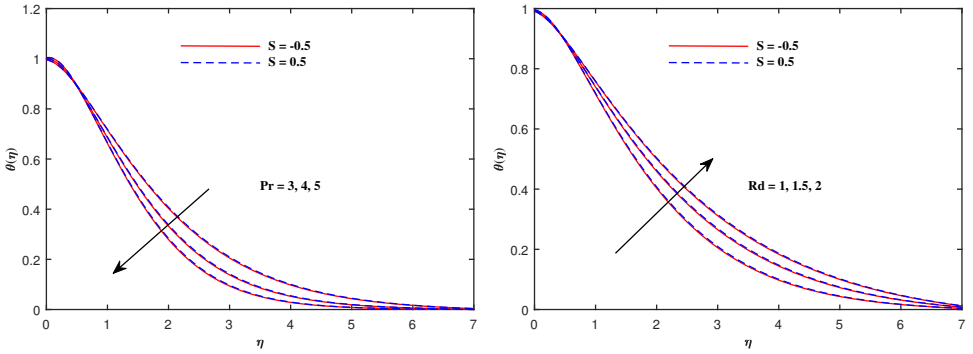

Figure 5. Temperature variation with Pr and Rd.

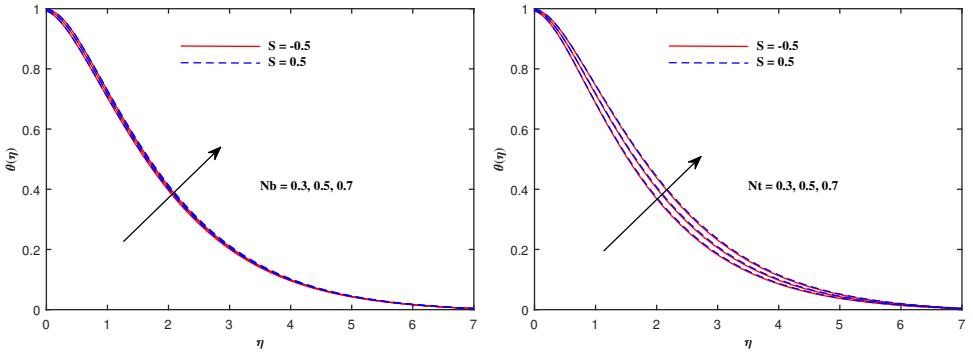

Figure 6. Temperature variation with Nb and Nt.

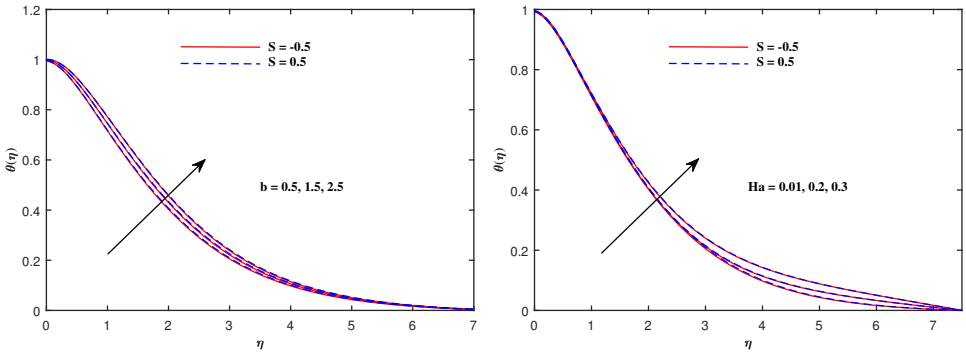

Figure 7. Temperature variation with b and Ha.

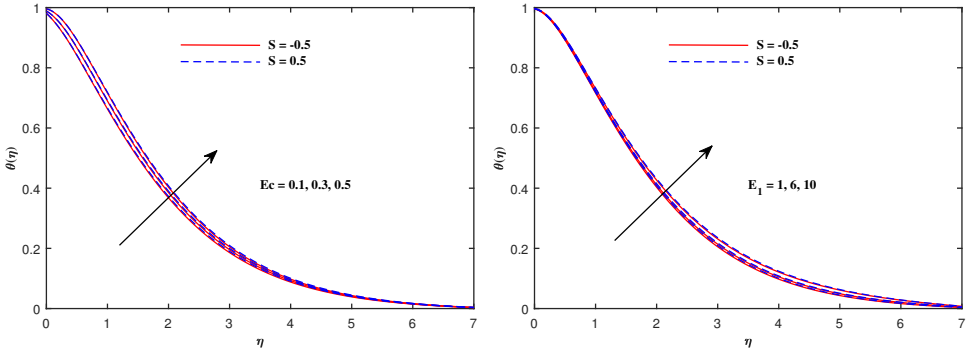

Figure 8. Temperature variation with Ec and E_1.

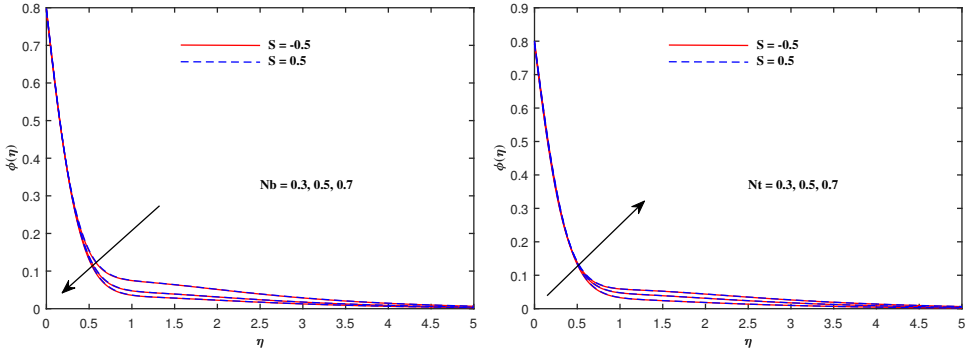

Figure 9. Concentration variation with Nb and Nt.

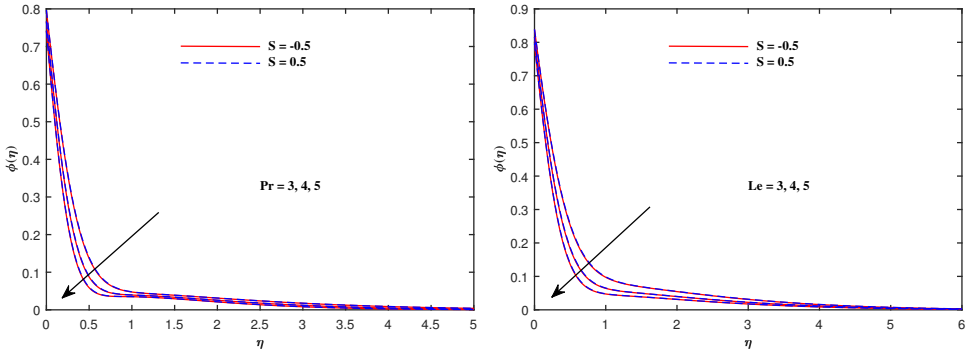

Figure 10. Concentration variation with Pr and Le.

Table 2. Results for $-f''(0)$.

Ha	S	Re	De	β	E_1	Kp	F_1^*	$-f''(0)$
0.01	0.5	0.5	0.5	0.1	1.0	0.1	0.3	1.0792
0.03								1.0780
0.05								1.0758
0.01	0.1							1.0191
	0.3							1.0486
	0.5							1.0792
	0.5	0.5						1.0792
		0.7						1.1109
		0.9						1.1440
		0.5	0.5					1.0792
			1.0					1.1610
			1.5					1.2522
			0.5	0.0				1.1889
				0.1				1.0792
				0.2				0.9685
				0.1	1.0			1.0792
					2.0			1.0790
					3.0			1.0788
					1.0	0.1		1.0792
						0.2		1.1209
						0.3		1.1608
						0.1	0.1	1.0359
							0.2	1.0579
							0.3	1.0792

Table 3. Results for $-\theta'(0)$.

Rd	Pr	b	Ec	Ha	E_1	Nt	Nb	$-\theta'(0)$
1.0	3.0	0.5	0.5	0.01	1.0	0.5	0.5	0.0408
2.0								0.0831
3.0								0.0985
1.0	1.0							0.1063
	2.0							0.0773
	3.0							0.0408
	3.0	0.1						0.0517
		0.3						0.0462
		0.5						0.0408
		0.5	0.1					0.1875
			0.3					0.1145
			0.5					0.0408
			0.5	0.01				0.0408
				0.03				0.0416
				0.05				0.0429
				0.01	1.0			0.0408
					3.0			0.0403
					5.0			0.0387
					1.0	0.1		0.0921
						0.3		0.0647
						0.5		0.0408
						0.5	0.1	0.1075
							0.3	0.0709
							0.5	0.0408

Table 4. Results for $-\phi'(0)$.

Le	Pr	Nb	Nt	$-\phi'(0)$
3.0	3.0	0.5	0.5	1.6124
4.0				1.8410
5.0				2.0313
5.0	1.0			1.1343
	2.0			1.6545
	3.0			2.0313
	3.0	0.1		2.2199
		0.3		2.0662
		0.5		2.0313
		0.5	0.1	1.9574
			0.3	1.9925
			0.5	2.0313

5. Conclusions

The electro-magnetohydrodynamic boundary layer transport of Maxwell Sutterby nanofluid with multi-slip conditions across an extending sheet is explored. A brief description of the significant findings is as follows:

- The velocity gradient enhanced as the magnitude of β, E_1 and Ha elevated, although it dropped significantly as the valuation of Kp and F_1^* extended.
- It is worth mentioning that the velocity field uplifted for De and Re when Sutterby parameter S take negative values and decrease when Sutterby parameter is positive.
- Temperature goes up if the magnitudes of Rd, Nb, Nt, b, Ha, Ec as well as E_1 upsurge, whereas it drops as the valuation of Pr grows.
- The concentration distribution for Nb, Pr and Le reveals a declining trend while upsurge with higher Nt.
- Skin friction reduces when Ha and β takes higher values. Furthermore, it escalates in direct proportion to S, $4Re$, De, kp and F_1^*.
- The Nusselt number explicitly elevated as the values of Rd, Ha as well as Nb improved. The inverse attitude of Pr, b, Ec, E_1 and Nt is revealed.
- The Sherwood quantity falls for Pr as well as Nb while surging for Le and Nt.

Author Contributions: Conceptualization, I.S.; methodology, I.S. and H.M.A.; software, W.W.; validation, A.A.A.M.; formal analysis, M.M.M.J.; investigation, M.M.M.J. and Z.M.; resources, Z.M.; data curation, S.A.; writing—original draft preparation, S.A.; writing—review and editing, W.W. and A.A.A.M.; visualization, H.M.A.; supervision, I.S.; funding acquisition, M.M.M.J. and Z.M. All authors have read and agreed to the published version of the manuscript.

Funding: This research received no external funding.

Data Availability Statement: Not applicable.

Acknowledgments: This Research was supported by Taif University Researchers Supporting Project Number (TURSP-2020/48), Taif University, Taif, Saudi Arabia.

Conflicts of Interest: The authors declare no conflict of interest.

Nomenclature

List of Symbols

u, v	velocity components
x, y	Cartesian coordinates
S	flow deportment index
b_c^2	consistency index
σ_m	magnetic permeability
E_f	electric field strength

C_F^*	Forchheimer quantity
T	temperature
C	solutal density
k_1	thermal conductivity
C_p	specific heat
τ_1	heat relaxation time
q_r	radiative heat flux
g	gravity acceleration
S	deportment index
b^2	consistency index
Pr	Prandtl number
Re_x	Reynolds number
h_f	heat transfer coefficient
D_B	Brownian motion
De	Sutterby Deborah number
Nr	buoyancy ratio
D_T	thermophorsis coefficient
D_m	microorganism diffusivity coefficient
c_b	chemotaxis constant
W_c	swimming speed of cell
Rb	bio-convection Rayleigh number
Pr	Prandtl number
Gr	Grashoff number
M	magnetic field
Nb	Brownian motion parameter
Nt	thermophoresis parameter
Sc	Schmidt number
Le	Lewis number
Greek Symbols	
ρ	fluid density
λ_1	Maxwell parameter
α	thermal diffusivity
τ	ratio of heat capacity of nanofluid
Subscripts	
p	Nanoparticles
w	On the wall
∞	Ambient

References

1. Shende, T.; Niasar, V.J.; Babaei, M. Effective viscosity and Reynolds number of non-Newtonian fluids using Meter model. *Rheol. Acta* **2021**, *60*, 11–21. [CrossRef]
2. Chang, A.; Sun, H.; Vafai, K.; Kosari, E. Numerical analysis of flow and forced convection heat transfer of non-Newtonian fluid in a pipe based on fractional constitutive model. *Int. J. Numer. Methods Heat Fluid Flow* **2021**, *31*, 2680–2697. [CrossRef]
3. Bisht, M.; Patil, D.V. Assessment of multiple relaxation time-lattice Boltzmann method framework for non-Newtonian fluid flow simulations. *Eur. J. Mech.-B/Fluids* **2021**, *85*, 322–334. [CrossRef]
4. Abu-Bakr, A.; Abu-Nab, A. Vapour bubble growth within a viscous mixture non-Newtonian fluid between two-phase turbulent flow. *Int. J. Ambient. Energy* **2021**. [CrossRef]
5. Sohail, M.; Alrabaiah, H.; Nazir, U. Radiative flow of MHD non-Newtonian fluid by utilizing the updated version of heat flux model under Joule heating. *Heat Transf.* **2021**, *50*, 3407–3425. [CrossRef]
6. Turkyilmazoglu, M. Heat Transfer Enhancement Feature of the Non-Fourier Cattaneo–Christov Heat Flux Model. *J. Heat Transf.* **2021**, *143*, 094501. [CrossRef]
7. Ali, B.; Khan, S.A.; Hussein, A.K.; Thumma, T.; Hussain, S. Hybrid nanofluids: Significance of gravity modulation, heat source/sink, and magnetohydrodynamic on dynamics of micropolar fluid over an inclined surface via finite element simulation. *Appl. Math. Comput.* **2022**, *419*, 126878. [CrossRef]
8. Khan, S.A.; Ali, B.; Eze, C.; Lau, K.T.; Ali, L.; Chen, J.; Zhao, J. Magnetic dipole and thermal radiation impacts on stagnation point flow of micropolar based nanofluids over a vertically stretching sheet: Finite element approach. *Processes* **2021**, *9*, 1089. [CrossRef]
9. Sadiq, K.; Jarad, F.; Siddique, I.; Ali, B. Soret and radiation effects on mixture of ethylene glycol-water (50%-50%) based Maxwell nanofluid flow in an upright channel. *Complexity* **2021**, *2021*, 1–12. [CrossRef]

10. Ali, B.; Rasool, G.; Hussain, S.; Baleanu, D.; Bano, S. Finite element study of magnetohydrodynamics (MHD) and activation energy in Darcy–Forchheimer rotating flow of Casson Carreau nanofluid. *Processes* **2020**, *8*, 1185. [CrossRef]
11. Tayyab, M.; Siddique, I.; Jarad, F.; Ashraf, M.K.; Ali, B. Numerical solution of 3D rotating nanofluid flow subject to Darcy-Forchheimer law, bio-convection and activation energy. *S. Afr. J. Chem. Eng.* **2022**, *40*, 48–56. [CrossRef]
12. Ali, L.; Wang, Y.; Ali, B.; Liu, X.; Din, A.; Al Mdallal, Q. The function of nanoparticle's diameter and Darcy-Forchheimer flow over a cylinder with effect of magnetic field and thermal radiation. *Case Stud. Therm. Eng.* **2021**, *28*, 101392. [CrossRef]
13. Akram, J.; Akbar, N.S.; Tripathi, D. Blood-based graphene oxide nanofluid flow through capillary in the presence of electromagnetic fields: A Sutterby fluid model. *Microvasc. Res.* **2020**, *132*, 104062. [CrossRef]
14. Salahuddin, T.; Ali, Z.; Awais, M.; Khan, M.; Altanji, M. A flow behavior of Sutterby nanofluid near the catalytic parabolic surface. *Int. Commun. Heat Mass Transf.* **2022**, *131*, 105821. [CrossRef]
15. Hayat, T.; Masood, F.; Qayyum, S.; Alsaedi, A. Sutterby fluid flow subject to homogeneous–heterogeneous reactions and nonlinear radiation. *Phys. A Stat. Mech. Its Appl.* **2020**, *544*, 123439. [CrossRef]
16. Nawaz, M. Role of hybrid nanoparticles in thermal performance of Sutterby fluid, the ethylene glycol. *Phys. A Stat. Mech. Its Appl.* **2020**, *537*, 122447. [CrossRef]
17. Mir, N.A.; Farooq, M.; Rizwan, M.; Ahmad, F.; Ahmad, S.; Ahmad, B. Analysis of thermally stratified flow of Sutterby nanofluid with zero mass flux condition. *J. Mater. Res. Technol.* **2020**, *9*, 1631–1639.
18. Sabir, Z.; Imran, A.; Umar, M.; Zeb, M.; Shoaib, M.; Raja, M.A.Z. A numerical approach for two-dimensional Sutterby fluid flow bounded at a stagnation point with an inclined magnetic field and thermal radiation impacts. *Therm. Sci.* **2021**, *25*, 1975–1987. [CrossRef]
19. Mahdavi, M.; Sharifpur, M.; Meyer, J.P. Fluid flow and heat transfer analysis of nanofluid jet cooling on a hot surface with various roughness. *Int. Commun. Heat Mass Transf.* **2020**, *118*, 104842. [CrossRef]
20. Chakraborty, S.; Panigrahi, P.K. Stability of nanofluid: A review. *Appl. Therm. Eng.* **2020**, *174*, 115259. [CrossRef]
21. Esfe, M.H.; Esfandeh, S.; Hosseinizadeh, E. Nanofluid flooding for enhanced oil recovery in a heterogeneous two-dimensional anticline geometry. *Int. Commun. Heat Mass Transf.* **2020**, *118*, 104810. [CrossRef]
22. Swain, K.; Animasaun, I.L.; Ibrahim, S.M. Influence of exponential space-based heat source and Joule heating on nanofluid flow over an elongating/shrinking sheet with an inclined magnetic field. *Int. J. Ambient. Energy* **2021**. [CrossRef]
23. Ali, L.; Liu, X.; Ali, B.; Mujeed, S.; Abdal, S.; Khan, S.A. Analysis of magnetic properties of nano-particles due to a magnetic dipole in micropolar fluid flow over a stretching sheet. *Coatings* **2020**, *10*, 170. [CrossRef]
24. Abdal, S.; Ali, B.; Younas, S.; Ali, L.; Mariam, A. Thermo-diffusion and multislip effects on MHD mixed convection unsteady flow of micropolar nanofluid over a shrinking/stretching sheet with radiation in the presence of heat source. *Symmetry* **2020**, *12*, 49. [CrossRef]
25. Ali, L.; Liu, X.; Ali, B.; Mujeed, S.; Abdal, S. Finite element analysis of thermo-diffusion and multi-slip effects on mhd unsteady flow of casson nano-fluid over a shrinking/stretching sheet with radiation and heat source. *Appl. Sci.* **2019**, *9*, 5217. [CrossRef]
26. Khan, J.A.; Mustafa, M.; Hayat, T.; Turkyilmazoglu, M.; Alsaedi, A. Numerical study of nanofluid flow and heat transfer over a rotating disk using Buongiorno's model. *Int. J. Numer. Methods Heat Fluid Flow* **2017**, *27*, 221–234. [CrossRef]
27. Ali, B.; Naqvi, R.A.; Nie, Y.; Khan, S.A.; Sadiq, M.T.; Rehman, A.U.; Abdal, S. Variable viscosity effects on unsteady mhd an axisymmetric nanofluid flow over a stretching surface with thermo-diffusion: Fem approach. *Symmetry* **2020**, *12*, 234. [CrossRef]
28. Sharma, R.; Hussain, S.; Raju, C.; Seth, G.; Chamkha, A.J. Study of graphene Maxwell nanofluid flow past a linearly stretched sheet: A numerical and statistical approach. *Chin. J. Phys.* **2020**, *68*, 671–683. [CrossRef]
29. Hussain, S.M.; Sharma, R.; Mishra, M.R.; Alrashidy, S.S. Hydromagnetic dissipative and radiative graphene maxwell nanofluid flow past a stretched sheet-numerical and statistical analysis. *Mathematics* **2020**, *8*, 1929. [CrossRef]
30. Abro, K.A.; Soomro, M.; Atangana, A.; Gómez-Aguilar, J. Thermophysical properties of Maxwell Nanofluids via fractional derivatives with regular kernel. *J. Therm. Anal. Calorim.* **2022**, *147*, 449–459. [CrossRef]
31. Ahmed, J.; Khan, M.; Ahmad, L. Radiative heat flux effect in flow of Maxwell nanofluid over a spiraling disk with chemically reaction. *Phys. A Stat. Mech. Its Appl.* **2020**, *551*, 123948. [CrossRef]
32. Shah, Z.; Alzahrani, E.; Jawad, M.; Khan, U. Microstructure and inertial characteristics of MHD suspended SWCNTs and MWCNTs based maxwell nanofluid flow with bio-convection and entropy generation past A permeable vertical cone. *Coatings* **2020**, *10*, 998. [CrossRef]
33. Ali, B.; Hussain, S.; Nie, Y.; Khan, S.A.; Naqvi, S.I.R. Finite element simulation of bioconvection Falkner–Skan flow of a Maxwell nanofluid fluid along with activation energy over a wedge. *Phys. Scr.* **2020**, *95*, 095214. [CrossRef]
34. Alsaedi, A.; Alsaadi, F.; Ali, S.; Hayat, T. Stagnation point flow of Burgers' fluid and mass transfer with chemical reaction and porosity. *J. Mech.* **2013**, *29*, 453–460. [CrossRef]
35. Ibrahim, W.; Negera, M. MHD slip flow of upper-convected Maxwell nanofluid over a stretching sheet with chemical reaction. *J. Egypt. Math. Soc.* **2020**, *28*, 7. [CrossRef]
36. Haider, S.M.A.; Ali, B.; Wang, Q.; Zhao, C. Stefan Blowing Impacts on Unsteady MHD Flow of Nanofluid over a Stretching Sheet with Electric Field, Thermal Radiation and Activation Energy. *Coatings* **2021**, *11*, 1048. [CrossRef]
37. Yahya, A.U.; Salamat, N.; Habib, D.; Ali, B.; Hussain, S.; Abdal, S. Implication of Bio-convection and Cattaneo-Christov heat flux on Williamson Sutterby nanofluid transportation caused by a stretching surface with convective boundary. *Chin. J. Phys.* **2021**, *73*, 706–718. [CrossRef]

38. Sajid, T.; Tanveer, S.; Sabir, Z.; Guirao, J. Impact of activation energy and temperature-dependent heat source/sink on Maxwell–Sutterby fluid. *Math. Probl. Eng.* **2020**, *2020*, 5251804. [CrossRef]
39. Abdal, S.; Siddique, I.; Alshomrani, A.S.; Jarad, F.; Din, I.S.U.; Afzal, S. Significance of chemical reaction with activation energy for Riga wedge flow of tangent hyperbolic nanofluid in existence of heat source. *Case Stud. Therm. Eng.* **2021**, *28*, 101542. [CrossRef]
40. Abdal, S.; Habib, U.; Siddique, I.; Akgül, A.; Ali, B. Attribution of Multi-slips and Bioconvection for Micropolar Nanofluids Transpiration Through Porous Medium over an Extending Sheet with PST and PHF Conditions. *Int. J. Appl. Comput. Math.* **2021**, *7*, 1–21. [CrossRef]
41. Abdal, S.; Siddique, I.; Alrowaili, D.; Al-Mdallal, Q.; Hussain, S. Exploring the magnetohydrodynamic stretched flow of Williamson Maxwell nanofluid through porous matrix over a permeated sheet with bioconvection and activation energy. *Sci. Rep.* **2022**, *12*, 1–12. [CrossRef] [PubMed]
42. Abdal, S.; Siddique, I.; Afzal, S.; Sharifi, S.; Salimi, M.; Ahmadian, A. An Analysis for Variable Physical Properties Involved in the Nano-Biofilm Transportation of Sutterby Fluid across Shrinking/Stretching Surface. *Nanomaterials* **2022**, *12*, 599. [CrossRef] [PubMed]